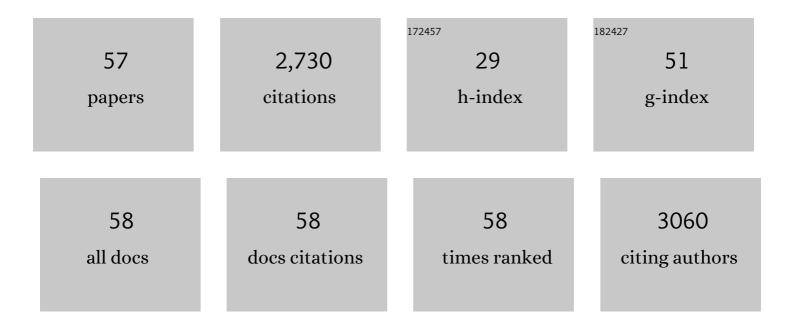
Sylvain Grangeon

List of Publications by Year in descending order

Source: https://exaly.com/author-pdf/4798059/publications.pdf Version: 2024-02-01



#	Article	IF	CITATIONS
1	Determination of Mn valence states in mixed-valent manganates by XANES spectroscopy. American Mineralogist, 2012, 97, 816-827.	1.9	256
2	Crystal structure of magnesium silicate hydrates (M-S-H): The relation with 2:1 Mg–Si phyllosilicates. Cement and Concrete Research, 2015, 73, 228-237.	11.0	139
3	Structure of nanocrystalline phyllomanganates produced by freshwater fungi. American Mineralogist, 2010, 95, 1608-1616.	1.9	138
4	Hydration Properties and Interlayer Organization of Water and lons in Synthetic Na-Smectite with Tetrahedral Layer Charge. Part 2. Toward a Precise Coupling between Molecular Simulations and Diffraction Data. Journal of Physical Chemistry C, 2011, 115, 1867-1881.	3.1	134
5	X-ray diffraction: a powerful tool to probe and understand the structure of nanocrystalline calcium silicate hydrates. Acta Crystallographica Section B: Structural Science, Crystal Engineering and Materials, 2013, 69, 465-473.	1.1	129
6	Zn sorption modifies dynamically the layer and interlayer structure of vernadite. Geochimica Et Cosmochimica Acta, 2012, 85, 302-313.	3.9	110
7	Modeling uranium(VI) adsorption onto montmorillonite under varying carbonate concentrations: A surface complexation model accounting for the spillover effect on surface potential. Geochimica Et Cosmochimica Acta, 2018, 220, 291-308.	3.9	102
8	Mercury speciation in a tropical soil association; Consequence of gold mining on Hg distribution in French Guiana. Geoderma, 2009, 153, 331-346.	5.1	93
9	Structure of nanocrystalline calcium silicate hydrates: insights from X-ray diffraction, synchrotron X-ray absorption and nuclear magnetic resonance. Journal of Applied Crystallography, 2016, 49, 771-783.	4.5	91
10	On the nature of structural disorder in calcium silicate hydrates with a calcium/silicon ratio similar to tobermorite. Cement and Concrete Research, 2013, 52, 31-37.	11.0	90
11	Modeling the Acid–Base Properties of Montmorillonite Edge Surfaces. Environmental Science & Technology, 2016, 50, 13436-13445.	10.0	89
12	Crystal structure of Ni-sorbed synthetic vernadite: a powder X-ray diffraction study. Mineralogical Magazine, 2008, 72, 1279-1291.	1.4	73
13	Distribution of Water in Synthetic Calcium Silicate Hydrates. Langmuir, 2016, 32, 6794-6805.	3.5	72
14	Modeling specific pH dependent sorption of divalent metals on montmorillonite surfaces. A review of pitfalls, recent achievements and current challenges. Numerische Mathematik, 2013, 313, 395-451.	1.4	71
15	Short-range and long-range order of phyllomanganate nanoparticles determined using high-energy X-ray scattering. Journal of Applied Crystallography, 2013, 46, 193-209.	4.5	70
16	Quantitative X-ray pair distribution function analysis of nanocrystalline calcium silicate hydrates: a contribution to the understanding of cement chemistry. Journal of Applied Crystallography, 2017, 50, 14-21.	4.5	68
17	Mineralogical characterization of individual growth structures of Mn-nodules with different Ni+Cu content from the central Pacific Ocean. American Mineralogist, 2015, 100, 2497-2508.	1.9	61
18	Mineralogical and isotopic record of biotic and abiotic diagenesis of the Callovian–Oxfordian clayey formation of Bure (France). Geochimica Et Cosmochimica Acta, 2011, 75, 2633-2663.	3.9	59

#	Article	IF	CITATIONS
19	Lichen and soil as indicators of an atmospheric mercury contamination in the vicinity of a chlor-alkali plant (Grenoble, France). Ecological Indicators, 2012, 13, 178-183.	6.3	59
20	Selenite Uptake by Ca–Al LDH: A Description of Intercalated Anion Coordination Geometries. Environmental Science & Technology, 2018, 52, 1624-1632.	10.0	58
21	Diurnal production of gaseous mercury in the alpine snowpack before snowmelt. Journal of Geophysical Research, 2007, 112, .	3.3	52
22	Atmospheric mercury incorporation in soils of an area impacted by a chlor-alkali plant (Grenoble,) Tj ETQq0 0 0 rg	BT /Overla 8.0	pck_{52} 10 Tf 50
23	Solid-state transformation of nanocrystalline phyllomanganate into tectomanganate: influence of initial layer and interlayer structure. Acta Crystallographica Section B: Structural Science, Crystal Engineering and Materials, 2014, 70, 828-838.	1.1	51
24	In situ interactions between Opalinus Clay and Low Alkali Concrete. Physics and Chemistry of the Earth, 2017, 99, 3-21.	2.9	44
25	Mineralogical transformations in polymetallic nodules and the change of Ni, Cu and Co crystal-chemistry upon burial in sediments. Geochimica Et Cosmochimica Acta, 2020, 282, 19-37.	3.9	44
26	Molecular-level understanding of metal ion retention in clay-rich materials. Nature Reviews Earth & Environment, 2022, 3, 461-476.	29.7	39
27	Evidence of Multiple Sorption Modes in Layered Double Hydroxides Using Mo As Structural Probe. Environmental Science & Technology, 2017, 51, 5531-5540.	10.0	38
28	Cryptomelane formation from nanocrystalline vernadite precursor: a high energy X-ray scattering and transmission electron microscopy perspective on reaction mechanisms. Geochemical Transactions, 2015, 16, 12.	0.7	37
29	Alteration of nanocrystalline calcium silicate hydrate (C-S-H) at pH 9.2 and room temperature: a combined mineralogical and chemical study. Mineralogical Magazine, 2015, 79, 437-458.	1.4	31
30	Hydration Properties and Interlayer Organization in Synthetic C-S-H. Langmuir, 2020, 36, 9449-9464.	3.5	28
31	In-situ determination of the kinetics and mechanisms of nickel adsorption by nanocrystalline vernadite. Chemical Geology, 2017, 459, 24-31.	3.3	26
32	Retention of arsenic, chromium and boron on an outcropping clay-rich rock formation (the Tégulines) Tj ETQq(0.0 rgBT	Overlock 10

33	Mineralogical and Isotopic Record of Diagenesis from the Opalinus Clay Formation at Benken, Switzerland: Implications for the Modeling of Pore-Water Chemistry in a Clay Formation. Clays and Clay Minerals, 2014, 62, 286-312.	1.3	25
34	Nucleation and growth of feitknechtite from nanocrystalline vernadite precursor. European Journal of Mineralogy, 2017, 29, 767-776.	1.3	21
35	The influence of natural trace element distribution on the mobility of radionuclides. The exemple of nickel in a clay-rock. Applied Geochemistry, 2015, 52, 155-173.	3.0	20
36	Effects of a thermal perturbation on mineralogy and pore water composition in a clay-rock: An experimental and modeling study. Geochimica Et Cosmochimica Acta, 2017, 197, 193-214.	3.9	19

3

Sylvain Grangeon

#	Article	IF	CITATIONS
37	Study of Iron-Bearing Dolomite Dissolution at Various Temperatures: Evidence for the Formation of Secondary Nanocrystalline Iron-Rich Phases on the Dolomite Surface. ACS Earth and Space Chemistry, 2017, 1, 442-454.	2.7	19
38	Retention and diffusion of radioactive and toxic species on cementitious systems: Main outcome of the CEBAMA project. Applied Geochemistry, 2020, 112, 104480.	3.0	16
39	Mechanistic and Thermodynamic Insights into Anion Exchange by Green Rust. Environmental Science & Technology, 2020, 54, 851-861.	10.0	16
40	Identification of montmorillonite particle edge orientations by atomic-force microscopy. Applied Clay Science, 2020, 186, 105442.	5.2	15
41	Iron and arsenic speciation in marine sediments undergoing a resuspension event: the impact of biotic activity. Journal of Soils and Sediments, 2014, 14, 615-629.	3.0	14
42	A novel and easy chemical-clock synthesis of nanocrystalline iron–cobalt bearing layered double hydroxides. Journal of Colloid and Interface Science, 2014, 434, 130-140.	9.4	13
43	Identification of nanocrystalline goethite in reduced clay formations: Application to the Callovian-Oxfordian formation of Bure (France). American Mineralogist, 2015, 100, 1544-1553.	1.9	13
44	Thermodynamic properties of chlorite and berthierine derived from calorimetric measurements. Physics and Chemistry of Minerals, 2014, 41, 603-615.	0.8	12
45	Thermodynamic and crystallographic model for anion uptake by hydrated calcium aluminate (AFm): an example of molybdenum. Scientific Reports, 2018, 8, 7943.	3.3	12
46	Deciphering mineralogical changes and carbonation development during hydration and ageing of a consolidated ternary blended cement paste. IUCrJ, 2018, 5, 150-157.	2.2	11
47	Competitive Adsorption Processes at Clay Mineral Surfaces: A Coupled Experimental and Modeling Approach. ACS Earth and Space Chemistry, 2022, 6, 144-159.	2.7	11
48	Influence of soil redox state on mercury sorption and reduction capacity. Science of the Total Environment, 2020, 707, 136069.	8.0	10
49	Evolution of iron minerals in a 100 years-old Technosol. Consequences on Zn mobility. Geoderma, 2017, 290, 19-32.	5.1	9
50	A quantitative and mechanistic model for the coupling between chemistry and clay hydration. Geochimica Et Cosmochimica Acta, 2020, 283, 124-135.	3.9	8
51	Weathering of an argillaceous rock in the presence of atmospheric conditions: A flow-through experiment and modelling study. Applied Geochemistry, 2018, 96, 252-263.	3.0	7
52	Dissolution kinetics of hydrated calcium aluminates (AFm-Cl) as a function of pH and at room temperature. Mineralogical Magazine, 2017, 81, 1245-1259.	1.4	6
53	The Nature of Manganese Oxides in Soils and Their Role as Scavengers of Trace Elements: Implication for Soil Remediation. Applied Environmental Science and Engineering for A Sustainable Future, 2020, , 399-429.	0.5	6
54	Constraints from sulfur isotopes on the origin of gypsum at concrete/claystone interfaces. Physics and Chemistry of the Earth, 2014, 70-71, 84-95.	2.9	5

#	Article	IF	CITATIONS
55	On the interaction between calcite and dolomite: Insights from gas and aqueous geochemistry and mineralogical characterization. Chemical Geology, 2021, 559, 119921.	3.3	5
56	Role of Carbonate Minerals in the Distribution of Trace Elements in Marine Clay Formations. Procedia Earth and Planetary Science, 2017, 17, 798-801.	0.6	3
57	Selenate Sorption by Hydrated Calcium Aluminate (AFm): Evidence for Sorption Reversibility and Implication for the Modeling of Anion Retention. ACS Earth and Space Chemistry, 2020, 4, 229-240.	2.7	3